Engineering Structures 288 (2023) 116235

Contents lists available at ScienceDirect

Engineering Structures

journal homepage: www.elsevier.com/locate/engstruct

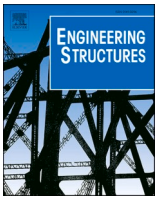

Explainable machine learning models for probabilistic buckling stress prediction of steel shear panel dampers

Shuling Hu [a,b], Wei Wang [a,*], Yongchang Lu [a]

[a] State Key Laboratory of Disaster Reduction in Civil Engineering & Department of Structural Engineering, Tongji University, Shanghai 200092, China
[b] JSPS International Research Fellow at Department of Architecture and Architectural Engineering, Kyoto University, Kyoto, Japan

ARTICLE INFO

Keywords:
Machine learning
Uncertainty
Probabilistic buckling stress
Steel shear panel damper
Global sensitivity analysis

ABSTRACT

Steel shear panel dampers are widely used as passive energy-dissipation devices in earthquake-resistant structures. The out-of-plane buckling stress of the core plate included in the steel shear panel damper is critical for obtaining the desired lateral force-resistant and hysteretic energy-absorbing capacities. However, the existing calculation method of buckling stress of the steel shear panel damper cannot well address the effects of the steel material's and geometries' inherent uncertainties. This paper intends to develop the probabilistic buckling stress prediction models of steel shear panel dampers using machine learning methods considering the steel material's and geometries' uncertainties. To this end, the nominal buckling stress prediction models are first developed using different machine learning algorithms based on finite element analysis results where the efficiency of the finite element models has been validated through test results. The analysis results confirm the highest accuracy of the artificial neural network (ANN) model. The SHapley Additive exPlanations (SHAP) and feature importance analysis methods are adopted for interpreting the developed prediction models. The analysis results indicate that the yielding stress of steel (f_y), the height-to-width ratio (α), the width-to-thickness ratio (β), and the initial imperfection (δ) show significant influences on the nominal buckling stress of the steel panel damper while the thickness of the core plate (t) shows negligible effects. The probabilistic buckling stress prediction models are further developed based on the trained ANN model considering the combined uncertainties of steel materials and geometries by the Latin hypercube sampling method. The efficiency of the developed probabilistic buckling stress prediction models is confirmed by capturing the probability density of the numerical simulation results. The global sensitivity analysis (GSA) method is introduced for investigating the influence of the design parameters on the discreteness of the probabilistic buckling stress. It has been found from the analysis results that the uncertainties of the yielding stress of steel (f_y) and the initial imperfection (δ) have significant influence, that of the height-to-width ratio (α) have limited influence, and that of the width-to-thickness ratio (β) and the thickness of the core plate (t) have negligible influence on the buckling stress of the steel panel damper. For practical application, the interactive software named "PBSSD" is developed and provided for predicting the probabilistic buckling stress by inputting the nominal design parameters of steel material and geometries.

1. Introduction

During Northridge and Kobe earthquakes, many steel structures failed with low ductility due to the brittle fracture of local structural members (e.g., beam-to-column connections), which is difficult, costly, and even impossible to be repaired. Since then, significant efforts have been made to improve the seismic performance of lateral force-resisting systems by enhancing ductility, hysteretic energy-dissipation capacity, and collapse-resistant capacity. Passive seismic control technology is one of the efficient ways to protect building structures suffering from earthquakes [1–6,77].

The steel shear panel damper (SSPD) is one kind of passive energy-dissipation device and has been widely used in engineering structures located in seismic regions [7]. SSPDs are designed to resist the in-plane shear [8] and the shear-yielding behavior of the steel core plate develops plum hysteretic properties of SSPDs for absorbing the input energy of seismic events and efficiently protecting the building structures. Based on past experimental investigations [9,10], the out-of-plane buckling behavior of the core plates and premature failure of the plate boundary are two main issues that could deteriorate the energy-absorbing and

* Corresponding author at: Dept. of Structural Engineering, Tongji University, Shanghai, 200092, China.
E-mail addresses: shuling.hu.6@gmail.com (S. Hu), weiwang@tongji.edu.cn (W. Wang).

https://doi.org/10.1016/j.engstruct.2023.116235
Received 13 February 2023; Received in revised form 6 April 2023; Accepted 26 April 2023
Available online 6 May 2023

lateral force-resisting capacities. The premature failure of the plate boundary can be well controlled by properly designing the boundary elements. However, the out-of-plane buckling of the core plates is inevitable, especially in the plastic stage [11–13]. Based on the theory of the plate's shear buckling [14], the buckling stress can be used for quantifying the out-of-plane force-resistant capacity of the core plate where the core plate with higher buckling stress has the higher capacity to resist out-of-plane deformation. Accordingly, buckling stress is one key parameter for ensuring the excellent performance of SSPDs. For the elastic buckling behavior, the buckling stress is usually influenced by geometric parameters, including the height-to-width ratio, the width-to-thickness ratio, and initial imperfection. For the plastic buckling behavior, the buckling stress is also influenced by the material properties. In this case, the traditional theory of the elastic shear buckling plate [14] cannot accurately capture the buckling stress of the core plate.

Extensive past investigations have been made for calculating the buckling stress of shear plates. Gerard [15], Wang et al. [16,17], and Inoue [18] developed the theory of the plastic shear buckling plate for calculating the plastic buckling stress with the consideration of the hardening behavior of the material. However, the necessary theoretical hypothetical leads to the sacrifice of estimation's accuracy. Zhang et al. [19] experimentally investigated the shear buckling stress of low-yield-strength steel plates considering the plastic behavior. Jain et al. [20] experimentally investigated the post-yield buckling behavior of aluminum shear panels. These studies confirmed that physical tests can accurately estimate the buckling stress of the shear plate, but it is impossible to conduct the tests for all potential shear plates. Alternatively, the finite element (FE) method can also accurately capture the buckling stress of the shear plate with a low cost. Many parametric numerical studies have been conducted to investigate the buckling behavior of shear plates based on advanced FE models [21–23]. Nevertheless, the influence of the inherent uncertainties of material, geometries, and initial imperfection on the buckling stress was not well addressed in past investigations. Moreover, it is costly and time-consuming to investigate the influence of the uncertainties of material, geometries, and initial imperfection through physical tests and FE models because thousands of samples are usually needed for a specific design case.

Machine learning technology has been widely used in civil engineering in recent years for addressing highly nonlinear issues [24–30]. Jeon et al. [31] developed machine learning models to accurately predict the strength of reinforced concrete connections. Le et al. developed machine learning models for predicting the strength of concrete-filled steel tubular structural members [32,33]. Mangalathu et al. developed different machine-learning models using various algorithms for predicting the strength of reinforced concrete beams [34], flab slabs [35], and shear walls [36]. These past investigations have confirmed that well-trained machine-learning models can rapidly predict the desired results with excellent accuracy. Nevertheless, the influence of the steel material's and geometries' uncertainties on the strength prediction of structural members was not well considered in past investigations. For addressing this issue, Hu et al. [37] propose a two-stage machine learning framework and develop the probabilistic strength prediction model of RHS-CHS T-joints. The analysis results indicate that the developed probabilistic strength prediction model can accurately capture the strength of RHS-CHS T-joints considering the uncertainties of material and geometries, confirming the efficiency of the proposed framework [37]. However, the research on developing the machine learning models for predicting the probabilistic buckling stress of SSPD considering the steel material's and geometries' uncertainties is limited.

For filling the aforementioned research gap, this paper intends to develop the explainable probabilistic buckling stress prediction models of SSPDs using existing machine learning algorithms considering the uncertainties of the steel material and geometries. To this end, the nominal buckling stress prediction models are first developed using different machine learning algorithms based on analysis results where the efficiency of the FE models will be validated through test results. The SHapley Additive exPlanations (SHAP) and feature importance analysis methods are adopted for interpreting the developed prediction models. The probabilistic buckling stress prediction models are further developed considering the combined uncertainties of steel materials and geometries by the Latin hypercube sampling (LHS) method. The global sensitivity analysis (GSA) method is introduced for investigating the influence of the design parameters on the discreteness of the probabilistic buckling stress. For practical application, the interactive software named "PBSSD" is developed and provided for predicting the probabilistic buckling stress of SSPDs by inputting the nominal design parameters of steel material and geometries.

2. Nominal buckling stress prediction model of SSPDs

2.1. FE model of SSPDs

As shown in Fig. 1, the considered SSPD consists of two connectors, one core plate, and two flange plates. These components are connected by welding. The FE models of the considered SSPDs were developed through ABAQUS software [38]. Three-dimensional solid elements with reduced integration points (i.e., C3D8R) were used for modeling the SSPDs. The tie constraint was used for connecting the core plate to the boundary members. The elements of core plates and flange plates were discretized into three layers to accurately capture the buckling behavior. As shown in Fig. 2(b), two reference points (i.e., RP-A and RP-B) were established and coupled with the top and bottom surfaces of the SSPD. The loads and boundary conditions were applied by the reference points. All degrees of freedom were fixed for the bottom surface of the SSPD and the lateral displacement was applied to the top surface to simulate the shear behavior of the SSPD. The static general was used for loading the model. The large deformations were considered in the numerical simulation. The Chaboche combined hardening model was used to simulate the nonlinear behavior of steel material. The initial imperfection was considered based on the first buckling mode of the SSPD. The maximum value of the initial imperfection was represented using the parameter δ. Different δ values will be considered for investigating the influence of initial imperfection on the buckling stress of the SSPD in the following sections.

The verification of the introduced FE modeling method of SSPDs was evaluated based on the tests conducted by Inoue [18]. Table 1 shows the geometries of the tested SSPDs, where d, l, t are the width, height, and thickness of the core plate, respectively, and t_f and c are the thickness and width of the flange plate. α and β are the height-to-width ratio and width-to-thickness ratio, respectively, and are defined in Eqs. (1) and (2), receptively. Fig. 2(a) shows the sketch of the test arrangement in the reference [18]. The shear force F was applied through the actuator at the top of the specimen. Fig. 2(d) shows the test results provided in [18], where U is the shear deformation (see Fig. 2(a)) and F_y and U_y are the yield shear force and corresponding displacement, respectively. The parameters of the Chaboche combined hardening model were determined based on the test results of the steel coupon in the reference [18]. As shown in Fig. 2(c), the Chaboche combined hardening model can well capture the nonlinear behavior of the steel used in the considered damper. Fig. 2 compares the numerical simulation results and the test results. It can be observed from Fig. 2 that numerical simulation results can match well with the test results for all considered test specimens. In particular, the strength deterioration of the SSPD specimens caused by out-of-plane buckling behavior can be well captured by the developed FE models, confirming that the introduced numerical modeling method can accurately simulate the nonlinear behavior of the SSPD under shear forces.

$$\alpha = \frac{l}{d} \tag{1}$$

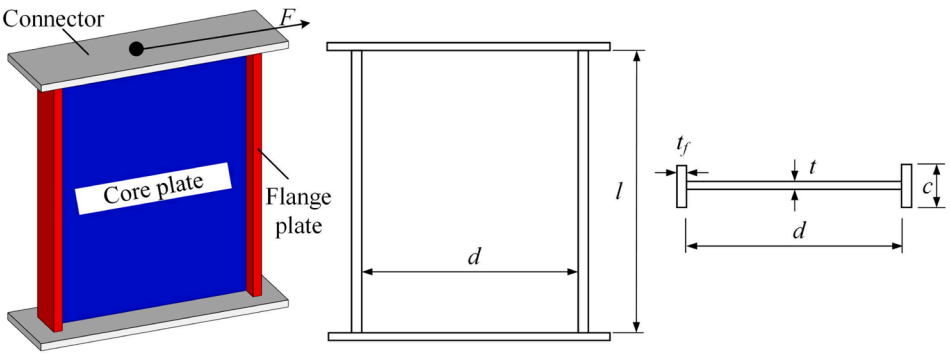

Fig. 1. Steel shear panel damper.

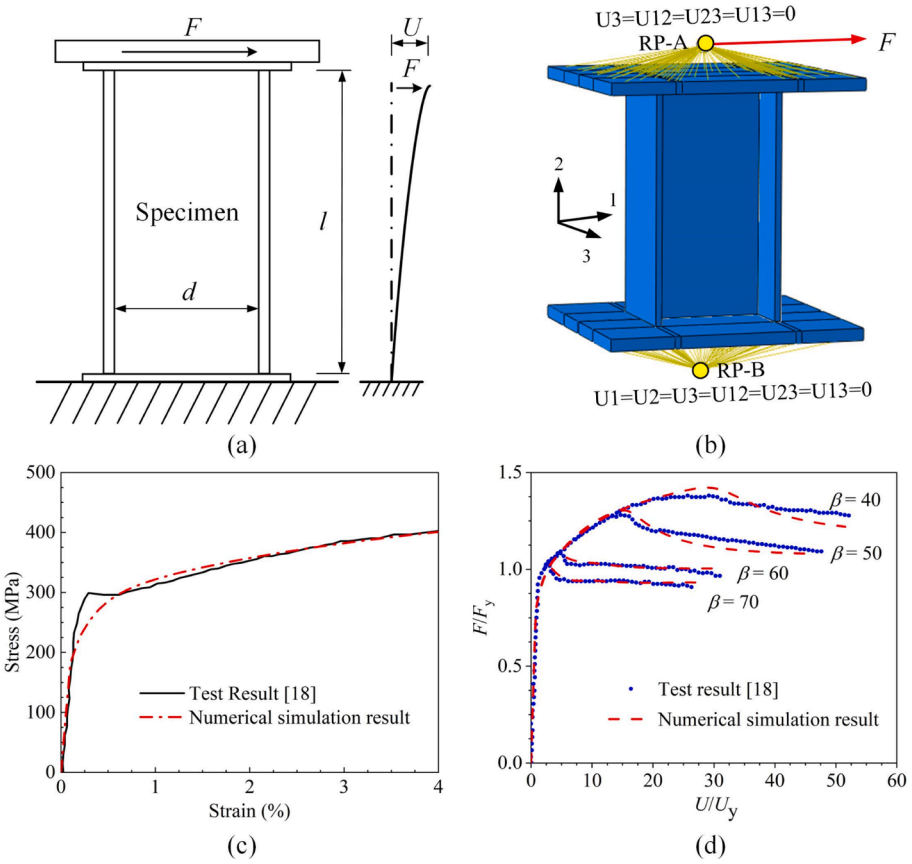

Fig. 2. Test and numerical simulation of steel shear panel dampers: (a) sketch of the tested specimen in [18], (b) sketch of the numerical model, (c) simulation of the nonlinear behavior of steel, and (d) buckling stress obtained from tests and numerical simulations.

Table 1
Geometries of the tested MSPDs [18].

d (mm)	c (mm)	t (mm)	t_f (mm)	β	c/t_f	l (mm)	α
180	168	4.44	11.74	40.5	14.4	360	2.0
225	204	4.44	11.74	50.7	17.4	450	2.0
270	176	4.44	15.36	60.8	11.4	540	2.0
315	208	4.44	15.36	71.0	13.6	630	2.0

$$\beta = \frac{d}{t} \tag{2}$$

2.2. Definition of buckling stress

Past investigations [10] indicate that before the development of out-of-plane buckling behavior, the core plate in the SSPD can achieve pure-shear conduction where the shear stress in the core plate is uniform. After the out-of-plane buckling behavior occurs, the shear stress in the core plate becomes nonuniform because of the local bending deformation of the core plate [40]. Accordingly, the out-of-plane buckling behavior introduces the nonuniform shear stress and out-of-plane deformation of the core plate. Based on the investigation by Zhou et al. [41], the out-of-plane deformation can be used for evaluating the occurrence of out-of-plane buckling behavior of the core plate in the

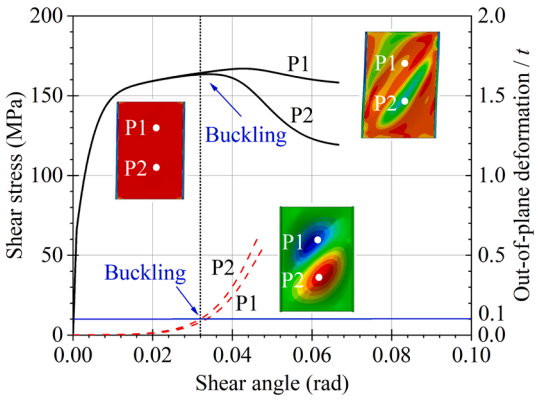

Fig. 3. Shear stress vs shear angle curves of the SSPD.

SSPD. Fig. 3 shows the shear stresses of two positions, which were randomly selected, in the core plate and the out-of-plane deformation of the core plate under shear loading. When the maximum out-of-plane deformation is larger than 0.1 times the core plate thickness, the shear stresses of the selected two positions become different, indicating the occurrence of the out-of-plane buckling behavior. The shear stress where the maximum out-of-plane deformation is equal to 0.1 times the core plate thickness is defined as the buckling stress of the SSPD [41].

2.3. Database of the buckling stress

Parametrically numerical simulation was conducted in this section using the verified FE models to generate the database of the buckling stress of SSPDs. The buckling stress of the SSPD is influenced by the material, geometries, and initial imperfection. The nominal yielding stress of steel (f_y), the thickness of the core plate (t), the height-to-width ratio (α), the width-to-thickness ratio (β), and the initial imperfection (δ) were considered as the key design parameters of the SSPD [8,9,43–48]. Table 2 shows the considered values of the design parameters. The geometries of the boundary members (i.e., c and t_f) were set as large enough values for ensuring a strong boundary. It is worth noting that these design values shown in Table 2 were selected based on the past tests of SSPDs for covering the potential practical design cases [8,9,43–48]. As shown in Table 2, 9 values of f_y, 8 values of α, 10 values of β, 5 values of t, and 9 values of δ were considered for developing the database of the buckling stress of SSPDs, and 32,400 simulation results were achieved. If the training database and testing database are directly obtained from this database, some design parameters in the testing database may be the same as that in the training database. For example, the combination [f_y = 100 MPa, t = 6 mm, α = 0.6, β = 30, and δ = 0.002 t] is the training data and the combination [f_y = 100 MPa, t = 6 mm, α = 0.6, β = 60, and δ = 0.002 t] may be the test data. 4 design parameters in the training and testing datasets have the same values. In this case, even though the developed machine models can achieve excellent accuracy, the accuracy is not credible. Thus, the 32,400 simulation results were used as the training dataset. To reliably avoid the overfitting of the machine learning model, additional 9,700 numerical models were established and analyzed for developing the test dataset, where the design values of f_y, α, β, t, and δ were randomly selected and were not included in Table 2 for ensuring the test dataset's credibility.

Table 2
Considered values of design parameters.

Parameters	f_y (MPa)	α	β	t (mm)	δ (mm)
Number	9	8	10	5	9
Value	80, 100, 120, 140, 160, 180, 200, 225, 250	0.5, 0.6, 0.7, 0.8, 1.0, 1.5, 2.0, 2.5	30, 35, 40, 45, 50, 60, 65, 70, 75, 80	3, 6, 9, 12, 15	0.001 t, 0.002 t, 0.005 t, 0.007 t, 0.01 t, 0.03 t, 0.05 t, 0.07 t, 0.1 t

2.4. Machine-learning models for predicting the nominal buckling stress of the SSPD

Various machine learning algorithms have been developed and adopted in civil engineering [24–30,37], for finding the most efficient machine learning algorithm for predicting the buckling stress of the SSPD, ten commonly used machine learning algorithms, including linear regression, ridge regression, lasso regression, K-nearest neighbor regression (KNN), Support Vector Regression (SVR), decision tree regression (DT), random forest regression (RF) [49], extreme gradient boosting (XGBoost) [50–52], adaptive boosting (AdaBoost), and artificial neural network (ANN) [53,54], were used in this section to develop the prediction models of the nominal buckling stress of the SSPD based on the 32,400 training data. The coefficient of determination (R^2), which can be calculated through Eq. (3), and the root mean square error (*RMSE*), which can be calculated through Eq. (4), were adopted for evaluating the effectiveness of the developed machine learning models based on the 9,700 test data. The following briefly introduces the used machine learning algorithms and the corresponding hyperparameters:

(1). Linear regression.

Linear regression is the simplest machine learning algorithm. Associations between the input and output variables were assessed by linear relationships [55]. The linear regression algorithm has no hyperparameters.

(2). Lasso regression.

The lasso regression overcomes the over-fitting problem of linear regression by adding a regularization term to the cost function [56]. This algorithm uses the absolute value of the weight as the regularization term.

(3). Ridge regression.

Unlike the lasso regression, ridge regression uses the square of the weight as the regularization term [56]. The ridge regression algorithm aims to eliminate the weight of the least important features. The hyperparameter α in this algorithm was set as 1.0 based on the research by Mangalathu et al. [51] .

(4). KNN.

The KNN algorithm uses a similarity measure to predict the output [58]. This algorithm determines the model output based on the values of k data points that are close to the test data point. And k is the main hyperparameter in this algorithm. Based on the recommendation from [51], k was taken as 5 in this research.

(5). SVR.

The SVR algorithm fits data within a decision boundary [59]. The goal of the algorithm is to find the hyperplane containing the largest number of data points within a certain threshold. Based on the recommendation from [60], the hyperparameters (i.e., C and γ) are set as 600 and 0.001, respectively.

(6). DT.

The DT uses a tree-like decision structure for the classification of data points and their regression [61]. The source data is split into many

smaller subsets in a tree. This splitting process terminates when the maximum depth of the tree is reached or no split can be found to reduce the used metrics. According to Xu et al. [60], the minimum number of samples to split a leaf node for the decision tree was set as 30.

(7). RF.

The RF consists of many decision trees on different subsets of a given dataset. This algorithm can effectively reduce the risk of overfitting. The hyperparameters of this algorithm are selected according to the study in [51], where the number of estimators and the minimum number of samples to split a leaf node were set as 200 and 2, respectively.

(8). AdaBoost.

AdaBoost combines several weak learning models to develop a strong algorithm [61]. The algorithm adaptively reweights the data based on the previous performance of the weak learners, helping weak learners to perform better. For obtaining better performance, the number of estimators is set as 100 and the learning rate is set as 1.0 based on past investigations [51].

(9). XGBoost.

XGBoost is a modified form of the Gradient Boosted decision trees algorithm, which further uses the second-order Taylor expansion of the loss function [61]. The number of trees, the maximum depth of the trees, and the learning rate for XGBoost were set as 100, 4, and 0.3, respectively, based on prior studies [62].

(10). ANN.

The ANN is a mathematical model constructed by imitating the structure of the human brain, in which neurons are connected to form a network [63]. Each neuron unit is assigned a weight w. The ANN algorithm adjusts the weights of all nodes to minimize the error between the predicted value and the actual value. This algorithm has many hyperparameters to optimize during the training process. Based on past investigations [1], three hidden layers were adopted and 30 neurons were set in each hidden layer in this research.

$$R^2 = 1 - \frac{\sum_{i=1}^{n}(y_i - \widehat{y}_i)^2}{\sum_{i=1}^{n}(y_i - \overline{y})^2} \tag{3}$$

in which n, y_i, $\widehat{y}_i$, and $\overline{y}$ = test samples' number, the actual data, the prediction data, and the mean of the test data, respectively.

$$RMSE = \sqrt{\frac{1}{n}\sum_{i=1}^{n}(y_i - \widehat{y}_i)^2} \tag{4}$$

The performance of the trained machine learning models based on the ten algorithms is shown in Fig. 4, where the values of R^2 and $RMSE$ are also included. Note that the buckling stress of the SSPD was normalized in Fig. 4. As shown in Fig. 4, the ANN model can achieve the lowest value of $RMSE$ (i.e., 0.0094) and the highest value of R^2 (i.e., 0.9952) within the developed ten machine learning models, demonstrating the best effectiveness of the ANN algorithm in predicting the buckling stress of the SSPD. Moreover, the R^2 and $RMSE$ of the ANN model are close to 1.0 and zero, respectively, confirming the excellent accuracy and reliability of the developed ANN model. The developed ANN model will be used in the following sections.

3. Interpretation of the developed ANN model

SHAP is an effective solution based on the game theory to explain the supervised machine-learning models and has been widely used in past studies [36,64,65]. The additive feature attribution method, where the output is equal to the linear addition of inputs, is adopted in SHAP to

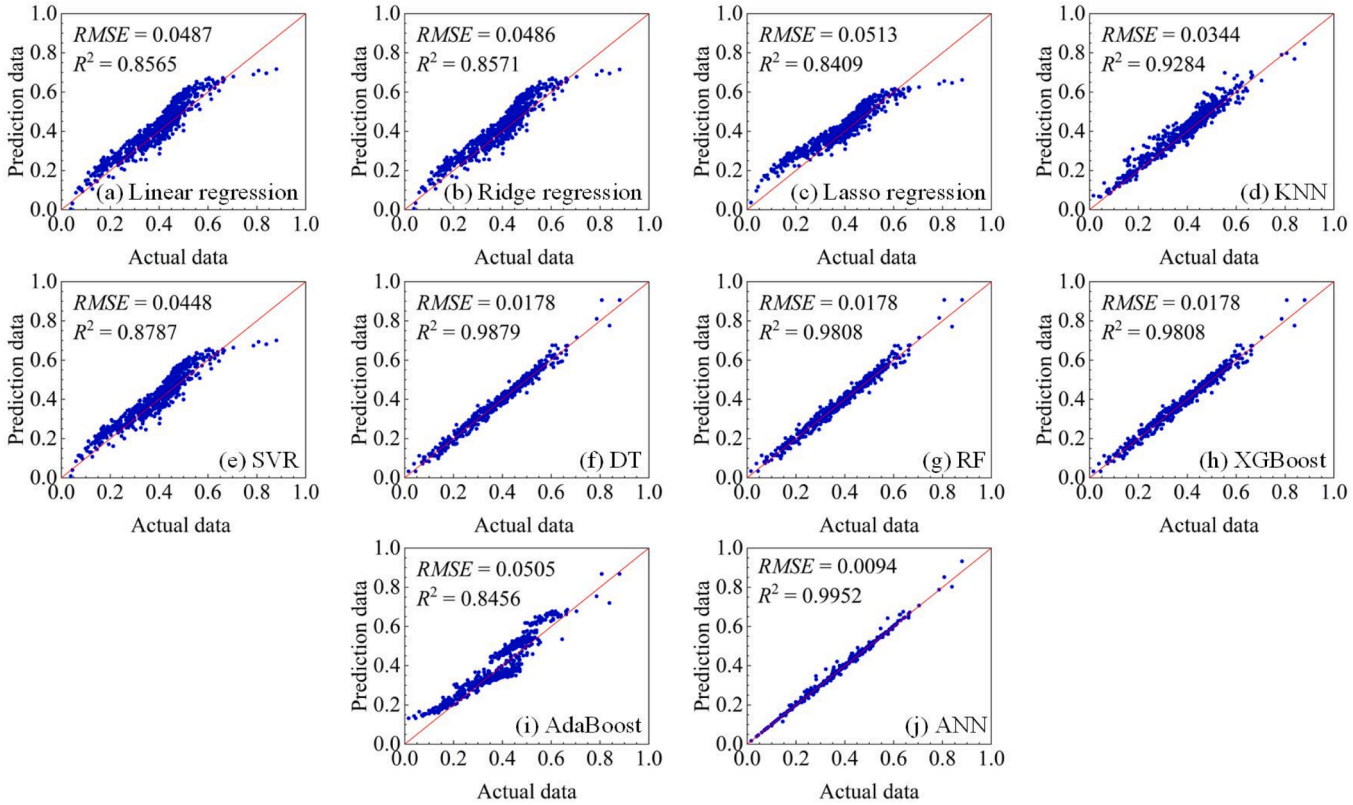

Fig. 4. Performance of the trained machine learning models.

develop the interpretable model. The explanation model based on the SHAP method can be modeled using Eq. (5). The detailed description of the SHAP method can be found in [36,64–66].

$$g(z) = \phi_0 + \sum_{j=1}^{M} \phi_j z_j \tag{5}$$

in which M = number of design parameters, ϕ_j = SHAP value related to the j^{th} design parameter, and z_j is the simplified design parameter.

Fig. 5 shows the SHAP value's distribution obtained based on the developed ANN model in Section 2.4. The magnitude of the SHAP value reflexes the importance of the design parameter, i.e., a larger absolute SHAP value indicates the higher importance of the design parameter. As shown in Fig. 5, the nominal yielding stress of steel (f_y), the height-to-width ratio (α), the width-to-thickness ratio (β), and the initial imperfection (δ) show significant influence on the buckling stress of the SSPD while the thickness of the core plate (t) shows negligible effects with the absolute SHAP values lower than 15. It is worth noting that the negligible effects of the thickness of the core plate (t) on the buckling stress of the steel shear panel damper were achieved because the width-to-thickness ratio (β) was considered as the design parameters in this research. The yielding stress of steel (f_y) shows the highest importance with the absolute SHAP value larger than 110. Fig. 6 shows the average absolute SHAP values of the considered design parameters. The average absolute SHAP values for f_y, α, β, t, and δ are 50.93, 10.54, 16.37, 1.52, and 11.94, respectively, confirming the highest importance of f_y and the lowest importance of t. α and δ show a similar influence on the buckling stress of the SSPD while β shows a higher influence than α and δ but a lower influence than f_y.

Moreover, it can also be found in Fig. 5 that with the increase of α, β, and δ, the coloring has a smooth decrease in shape values, and with the increase of f_y, the coloring has a smooth increase in shape values, confirmed by the partial dependent plots in Fig. 7. Although Figs. 5 and 7 show the same SHAP values, the deeper insight about the variation and spread of the SHAP value with the design parameters can be achieved by the partial dependent plots in Fig. 7. As shown in Fig. 7(a), 7(e), 7(j), 7(n), and 7(r), SHAP values tend to increase with the increase of f_y and decrease with the increase of α, β, and δ, indicating that the height-to-width ratio (α), the width-to-thickness ratio (β), and the initial imperfection (δ) have a negative relationship with the buckling stress of the SSPD while the yielding stress of steel (f_y) has the positive relationship with the buckling stress of the SSPD, which are consistent with the past investigations [67,68]. Moreover, the coloring in the partial dependent plots in Fig. 7 can reflect the interaction effects between different design parameters. For example, as shown in Fig. 7(j), when β greater than 55, a larger value of f_y leads to a smaller negative SHAP value for β, and when $\beta < 55$, a larger value of f_y leads to a larger positive SHAP value for β, indicating that f_y will emphasize the effect of β on the buckling stress of

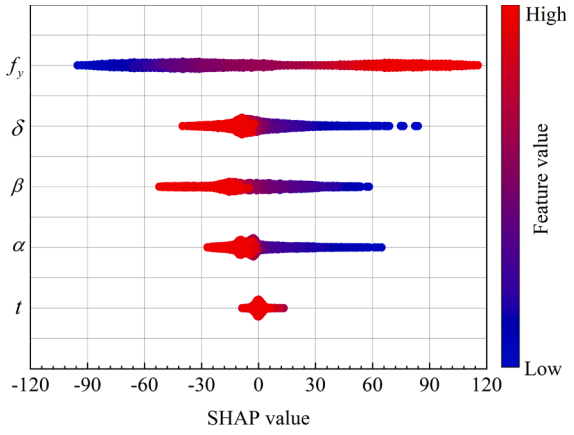

Fig. 5. SHAP values of the considered design parameters.

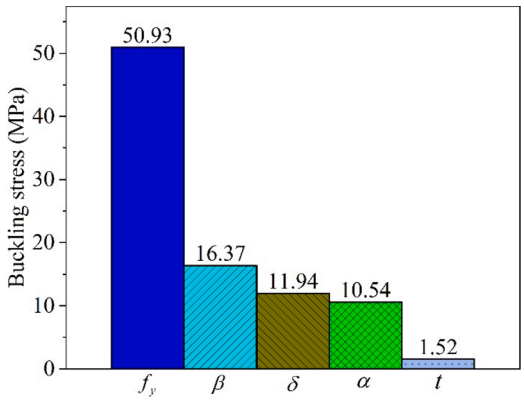

Fig. 6. Average absolute SHAP values of the considered design parameters.

the SSPD. As shown in Fig. 7(a), 7(b), 7(e), 7(j), and 7(r), f_y and α, f_y and β, and f_y and δ are dependent on the effects for the buckling stress of the SSPD.

The above analysis results on the global importance and dependence of the design parameters can provide sufficient references to the engineer or researcher for selecting the parameter values to design the SSPD.

4. Probabilistic buckling stress prediction model of SSPDs

The ANN model developed in Section 2 can only predict the specific buckling stress of the SSPD with the specific inputs of f_y, α, β, t, and δ. However, in practical construction, the actual buckling stress of the SSPD is usually different from the nominal value because of the inherent uncertainty of geometries and materials. In the traditional method, the inherent uncertainty of geometries and materials can be considered through numerical simulations, which is costly and time-consuming. It is worth noting that the developed ANN model can quickly give the buckling stress value of the SSPD by inputting f_y, α, β, t, and δ. The reliable accuracy of the ANN model developed in Section 2 brings a potential way for considering the influence of the inherent uncertainty of geometries and materials on the buckling stress of the SSPD by using the ANN model as the proxy model of FE models.

The LHS was used in this section for considering the inherent uncertainty of geometries and materials. The LHS, also called the stratified sampling method, was initially introduced by MacKay et al. [69]. This method can assure that the parameters used in the sampling process are non-overlapping. For creating multivariate samples with statistical distribution, the LHS is an effective way. Each random variable's distribution may be divided into m intervals with equal probability in the LHS. One point within each interval will be randomly selected, ensuring the selected samples can cover the distribution of the considered variable. Fig. 8 explains the sampling process using the LHS method, where two design parameters were considered. The sampling process includes the following steps:

1st step: Divide the range of each considered random parameter into m intervals based on the cumulative probability and ensure the probabilities for each interval are the same. In the example shown in Fig. 8, the distribution of the considered random parameter was divided into 5 intervals with the same probability of 0.2.

2nd step: Randomly chose a point in each interval of the considered variables. In Figs. 8, 10 points were selected for X_1 and X_2.

3rd step: The selected points for each considered variable should be associated randomly. 5 values of X_1 and 5 values of X_2 were randomly associated to generate 5 combinations of X_1 and X_2, as presented in Fig. 8 (c).

Based on the suggestion in JCSS [70], the normal distribution was used for describing the distribution of geometries of the SSPD, including the width d, height l, and thickness t of the core plate in the SSPD. Based

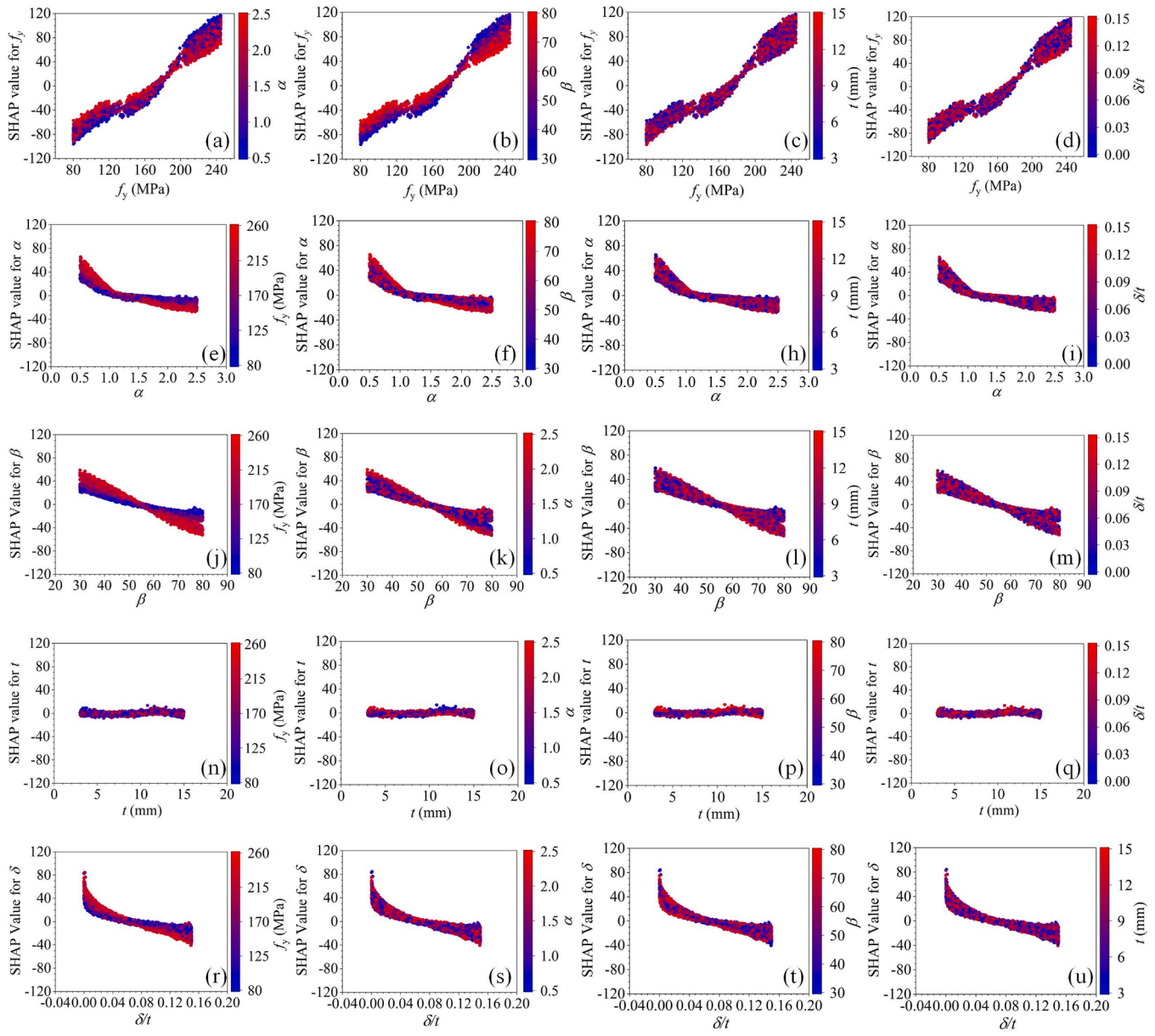

Fig. 7. SHAP dependence plot.

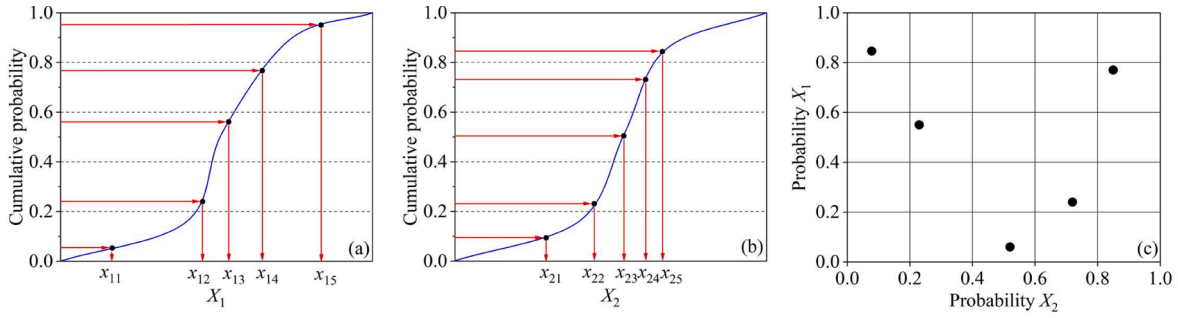

Fig. 8. Illustration of the steps of LHS.

on the investigation by Rahman et al. [71], $1000\delta/l$ follows the exponential distribution. According to the studies by Shi et al. [72], the yielding stress of steel f_y follows the normal distribution. Table 3 gives the parameters for developing the distribution functions of f_y, α, β, t, and δ.

The prediction models of the probabilistic buckling stress of the SSPD considering the inherent randomness of the geometries and materials can be following developed based on the ANN models and LHS method. The number of samples (i.e., the value of m in the LHS) may affect the prediction values of the probabilistic buckling stress of the SSPD. Four

Table 3
Distribution values of the considered design parameters.

Parameters	Distribution type	Distribution parameters
f_y	Normal	mean value = nominal design value, coefficient of variation = 0.05
d, l and t	Normal	mean value = nominal design value, coefficient of variation = 0.005
$1000\delta/l$	Exponential	$\lambda = 8.4993$

Table 4
Selected specific nominal values of design parameters.

Parameters	f_y (MPa)	α	β	t (mm)	Expect value of δ (mm)
Example 1	100.0	0.56	73.6	8.34	0.001 l/λ
Example 2	100.0	1.34	39.3	6.98	0.001 l/λ
Example 3	160.0	1.29	74.0	6.52	0.001 l/λ
Example 4	225.0	1.51	44.7	12.48	0.001 l/λ

examples were considered for investigating the influence of m. Note that the design parameters for the four examples in Table 4 are randomly selected. Table 4 shows the nominal values of f_y, α, β, t, and δ for the considered four examples. 10 values of m were considered for predicting the probabilistic buckling stress of the SSPD, including 200, 400, 600, 800, 1,000, 2,000, 4,000, 6,000, 8,000, and 10,000. Fig. 9shows the 5%, 25%, 50%, 75%, and 95% percentiles of the buckling stress with different m for the 4 considered cases. As shown in Fig. 9, when $m <$ 2,000, the considered percentiles of the predicted buckling stress changes with the increase of m, and when $m \geq$ 2,000, the change of m shows a negligible influence on the considered percentiles of the predicted buckling stress. These results indicate that $m \geq$ 2,000 can well capture the distribution of the buckling stress of the SSPD. m = 2,000 was used for developing the prediction models of the probabilistic buckling stress of the SSPD. For evaluating the effectiveness of the developed prediction models, the numerical models with the considered combination of f_y, α, β, t, and δ were also developed and analyzed. Fig. 10 shows the distribution of the buckling stress of the SSPD obtained from numerical simulations and prediction models. As shown in Fig. 10, the probability densities of the buckling stress obtained from the developed prediction model can well capture that obtained from FE simulation for all considered cases. The Two-sample Kolmogorov-Smirnov test (denoted as KS test) was further conducted to evaluate the efficiency of the developed machine learning prediction model. The KS test results show that the buckling stress of the SSPD obtained from numerical simulations and machine learning prediction models are from populations with the same distribution at the 1% significance level, validating the accuracy and reliability of the developed prediction model. For promoting the practical application of the developed prediction model, the software named "PBSSD" was developed and provided in the appendix for predicting the probabilistic buckling stress by inputting the nominal design parameters of steel material and geometries. Fig. 11 presents the software's user interface, where the probability density function (PDF) and cumulative distribution function (CDF) can be directly achieved by inputting the nominal values of f_y, α, β, t, and δ.

The developed prediction model of the probabilistic buckling stress of SSPDs was further compared to the existing calculation method for the shear buckling stress of steel. As shown in Eqs. (6) – (9), based on the experimental results of LYS160 steel with the yielding stress of 160 MPa, Zhang et al. [19] proposed the formula for calculating the shear buckling stress of steel considering the plastic behavior. It can be seen from Eqs. (6) – (9) that this calculation method cannot consider the influence of the initial imperfection and the inherent uncertainties of geometries and materials. 10 design cases were considered in this part and Table 5 shows the corresponding design parameters. Fig. 12 compares the shear buckling stress results obtained from the developed machine learning prediction model and Eqs. (6) – (9). As shown in Fig. 12, for case 1, the buckling stress obtained from Eqs. (6) – (9) can fall in the range from 5% to 95% quantiles of the buckling stress obtained through machine learning models. However, for the other cases, Eqs. (6) – (9) would overestimate or underestimate the shear buckling stress with significant deviation. These results confirm that the existing simplified formula cannot provide a reliable prediction of the shear buckling stress of steel

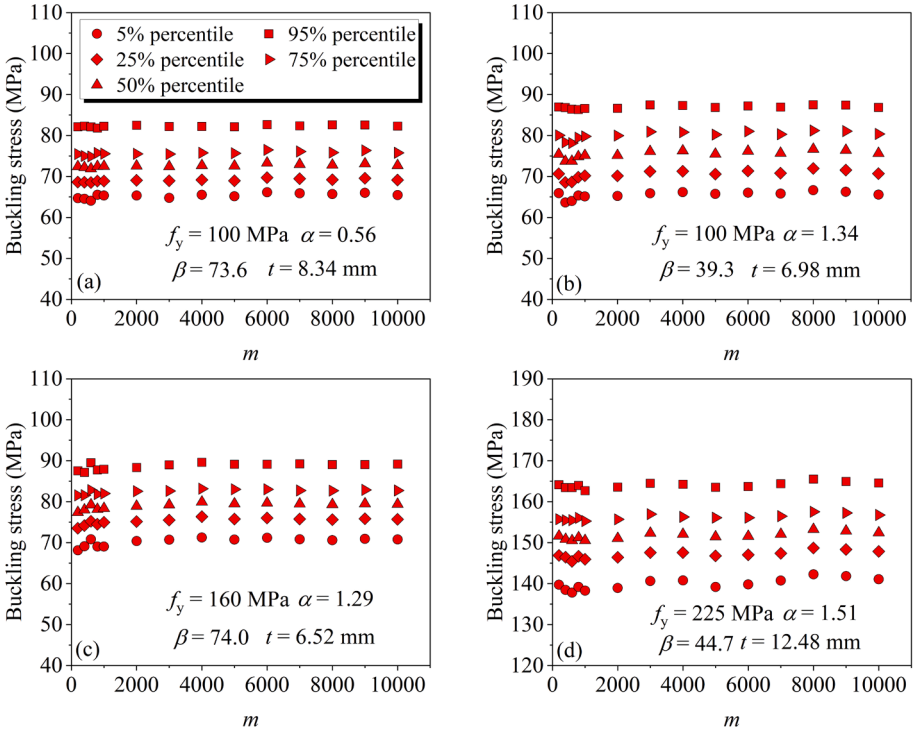

Fig. 9. Relationship between quantiles and sample quantity.

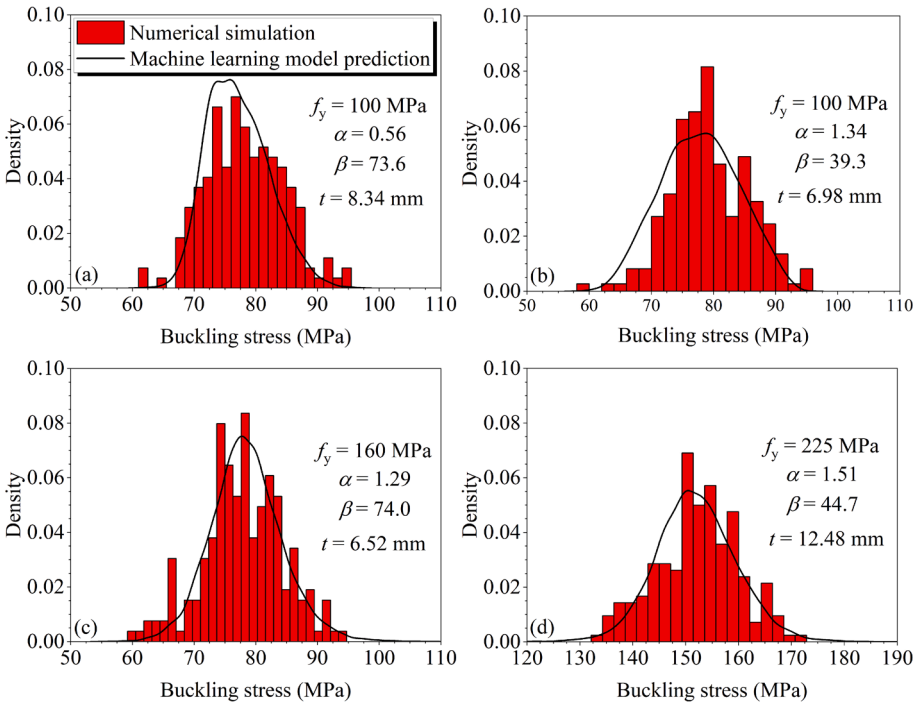

Fig. 10. Comparison between the probabilistic strength of the SSPDs obtained by numerical simulation and machine learning model.

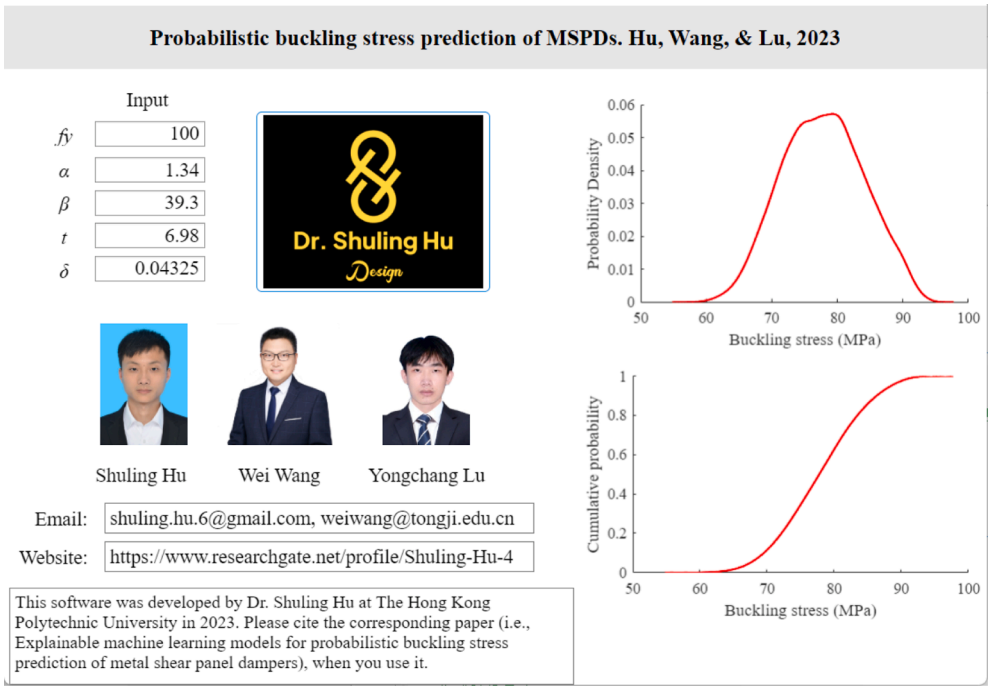

Fig. 11. User interface of PBSSD.

and it is important to consider the influence of the initial imperfection and the inherent uncertainties of geometries and materials on estimating the shear buckling stress of steel. Nevertheless, although the insufficient accuracy, the Eqs. (6) – (9) have better interpretability than the proposed machine learning prediction model, which needs to be considered in practical applications.

$$\tau_{cr} = K_p \frac{\pi^2 E_p}{12(1-\mu^2)} \left(\frac{t}{d}\right)^2 \tag{6}$$

$$K_p = 3.96 + \frac{2.24}{\phi^2} \text{ for } \phi = \frac{l}{d} > 1 \tag{7}$$

$$E_p = 31068 \cdot \gamma^{-0.552} \tag{8}$$

$$\gamma = 5200 \left(\frac{d}{t}\right)^{-1.85} \tag{9}$$

in which μ is the poison's ratio and was taken as 0.3 in this research.

Table 5
Design parameters for the design cases.

Case ID	f_y (MPa)	α	β	t (mm)	Expect value of δ (mm)	γ (x10^{-2}rad)	E_p (MPa)	K_p	τ_{cr} (MPa)
1	160	0.5	40	12.4	0.001 l/λ	5.65	11942.72	18.08	121.97
2	160	0.5	50	3.5	0.001 l/λ	3.74	14999.18	18.08	98.04
3	160	0.6	35	6.6	0.001 l/λ	7.23	10420.34	13.24	101.79
4	160	0.6	40	9.4	0.001 l/λ	5.65	11942.72	13.24	89.32
5	160	0.7	30	11.5	0.001 l/λ	9.62	8902.576	10.32	92.28
6	160	0.7	50	10.5	0.001 l/λ	3.74	14999.18	10.32	55.97
7	160	0.7	60	5.6	0.001 l/λ	2.66	18068.72	10.32	46.82
8	160	0.8	40	8.2	0.001 l/λ	5.65	11942.72	8.43	56.85
9	160	1.0	40	9.6	0.001 l/λ	5.65	11942.72	6.20	41.83
10	160	1.0	45	5.6	0.001 l/λ	4.54	13469.15	6.20	37.27

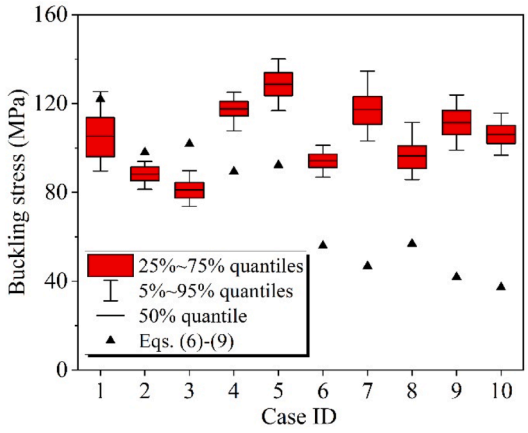

Fig. 12. Comparison between the prediction stress obtained from the machine learning model and Eqs. (6)-(9).

5. Global sensitive analysis

This section intends to investigate the influence of uncertainty of the design parameters (i.e., f_y, α, β, t, and δ) on the probabilistic buckling stress of the SSPD. The sensitivity analysis is an effective method for evaluating the influence of the uncertainty of inputs on the outputs. The sensitivity analysis method includes the local sensitivity analysis method (LSA) and global sensitivity analysis method (GSA). Compared to the LSA, GSA can well consider the interactions between the input variables and account for the full range of uncertainties of the input parameters. Various methods have been developed in past investigations [73] for conducting the GSA. Among these developed methods, Sobol's method [73–76] is one of the efficient and robust methods by characterizing the relationship between the inputs and outputs considering the input variable's high-order interactions. In Sobol's method [73–76], the output function $f(x)$ with an n-dimensional hypercube can be described as:

$$f(x) = f_0 + \sum_{i=1}^{n} f_1(x_i) + \sum_{i<j} f_{i,j}(x_i, x_j) + \cdots + f_{1,2,\cdots,n}(x_1, x_2, \cdots, x_n) \tag{10}$$

$$f_0 = \int_n f(x)dX; X = \{x_1, x_2, \cdots, x_n\} \tag{11}$$

The total variance can be calculated as:

$$D = \int [f(x)]^2 dX - f_0^2 \tag{12}$$

The biased variance can be obtained through:

$$D_{i_1,i_2,\cdots,i_s} = \int f^2_{i_1,i_2,\cdots,i_s} dx_{i_1} dx_{i_2} \cdots dx_{i_s} \tag{13}$$

The first-order sensitivity index can be calculated by:

$$S_i = \frac{D_i}{D} \tag{14}$$

in which S_i is the sensitivity mainly influenced by the input parameter x_i.

The total-order sensitivity index can be finally calculated through:

$$S_i^T = 1 - S_{\sim i} = 1 - \frac{D_{\sim i}}{D} \tag{15}$$

in which S_i^T is the sensitivity mainly caused by the input parameter x_i and the interactions between x_i and all the other input variables, and $D_{\sim i}$ is the variance caused by all the other input variables except for x_i. The LHS was used in this section to calculate S_i^T. 500 cases were analyzed, and the m was set as 100,000 in the LHS for each case to well consider the uncertainties of the design parameters (i.e., f_y, α, β, t, and δ).

Fig. 13 shows Sobol's index (i.e., S_i^T) for each considered design parameter. Note that a higher Sobol's index indicates that the uncertainty of the considered design parameter has a higher impact on the outputs (i.e., the probabilistic buckling stress of the SSPD). As shown in Fig. 13, the values of the Sobol's index for f_y and δ are much higher than that for the other parameters (i.e., α, β, and t), indicating that the buckling stress of the SSPD is significantly sensitive to the uncertainty of the yielding stress of steel f_y and the initial imperfection δ. Moreover, as shown in Fig. 13(c) and 13(d), the values of the Sobol's index for β and t are nearly equal to zero, demonstrating that the uncertainties of the width-to-thickness ratio (β) and the thickness of the core plate (t) have negligible influence on the buckling stress of the SSPD. In Fig. 13(b), the values of the Sobol's index for α are larger than zero but most of them are lower than 0.2, indicating that the uncertainties of the height-to-width ratio (α) have a non-negligible but limited influence on the buckling stress of the SSPD. These results confirm the importance of considering the uncertainties of geometries and materials while evaluating the buckling stress of the SSPD.

Fig. 14 plots the distribution of the buckling stress of the analyzed 500 cases. In Fig. 14, the red area represents the probabilistic buckling stress of the SSPD with the consideration of uncertainties of all design parameters and the blue area represents the probabilistic buckling stress without considering the concerned design parameter but with considering the uncertainties of the other design paraments. For example, in Fig. 14(a), the red area shows the probabilistic buckling stress considering the uncertainties of f_y, α, β, t, and δ, and the blue area only considers the uncertainty of α, β, t, and δ. As shown in Fig. 14(a), the blue area is smaller than the red area, especially for the cases with buckling stress higher than about 100 MPa, indicating that the uncertainties of the yielding stress of steel (f_y) have a significant influence on the buckling stress of the SSPD and this influence is more significant while the SSPD has larger buckling stress. It can also be observed from Fig. 14 (b) that the uncertainties of the height-to-width ratio α have an obvious influence on the buckling stress of the SSPD and the influence is more significant when the SSPD has larger buckling stress. As can be seen in Fig. 14(c) and 14(d), the difference between the red area and blue area can be ignored, indicating the negligible effects of the uncertainties of

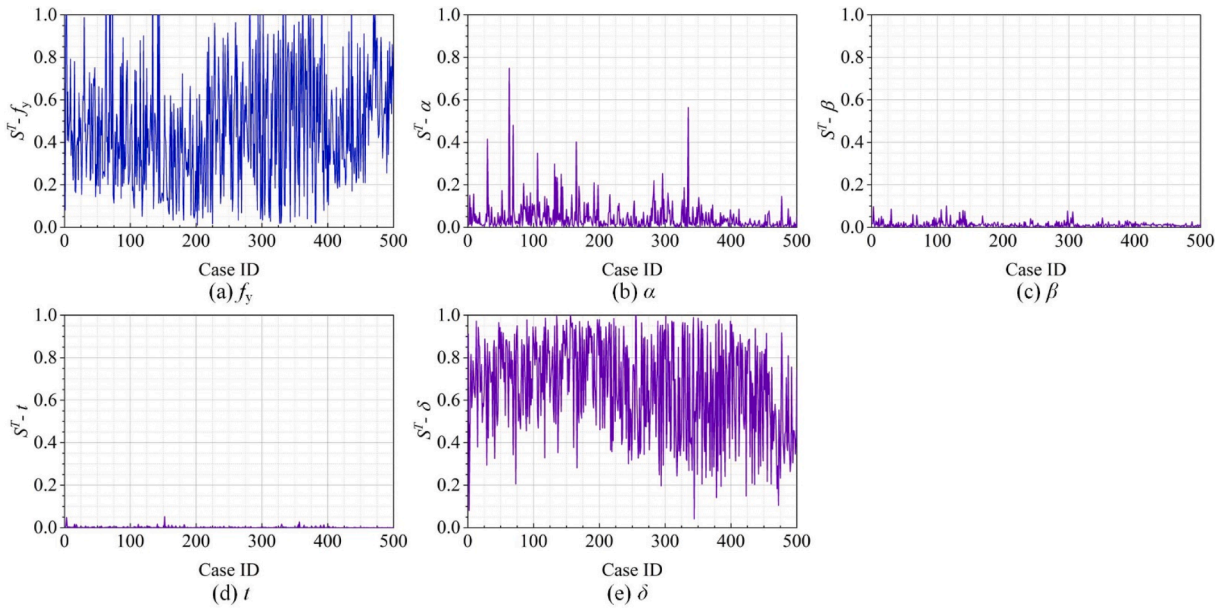

Fig. 13. Sobol's index for the considered design parameters.

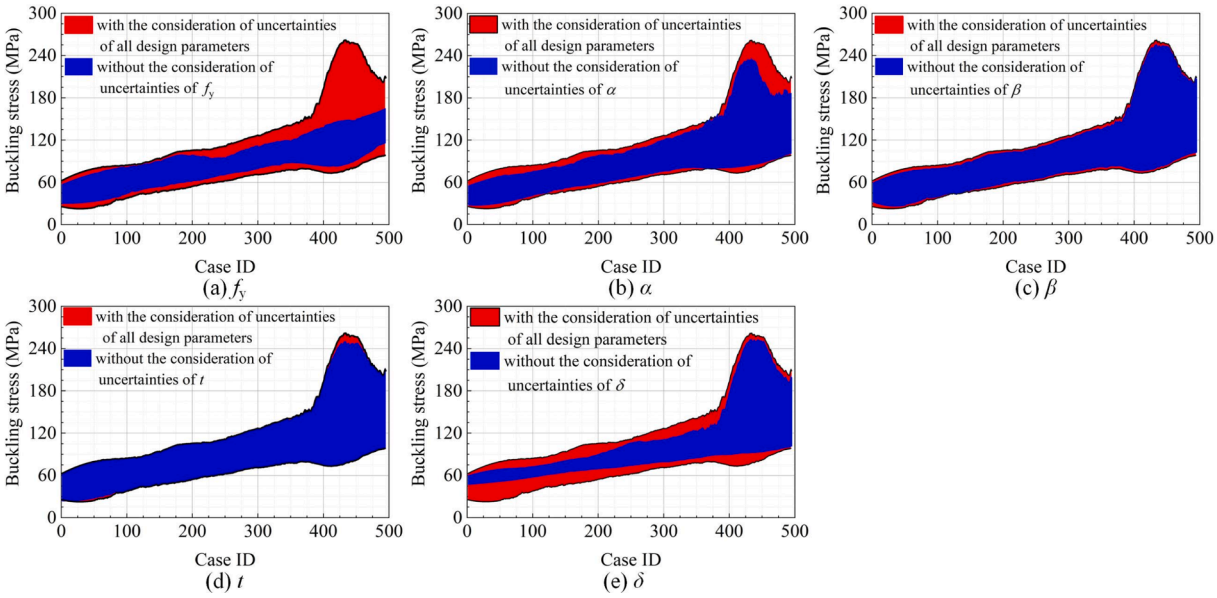

Fig. 14. Distribution of the buckling stress of the analyzed cases.

the width-to-thickness ratio (β) and the thickness of the core plate (t) on the buckling stress of the SSPD. Moreover, the difference between the red area and blue area becomes smaller with the increase of buckling stress, indicating that the uncertainty of the initial imperfection (δ) has significant effects on the buckling stress of the SSPD and this effect is more significant while the SSPD has lower buckling stress.

6. Conclusions

This paper developed the probabilistic buckling stress prediction models of steel shear panel dampers using machine learning methods considering the steel material's and geometries' uncertainties. The nominal buckling stress prediction models were first developed using different machine learning algorithms based on FE analysis results where the efficiency of the finite element models has been validated through test results. The elastic buckling, inelastic buckling, and shear-yielding behavior were well considered by the advanced numerical models. The SHAP and feature importance analysis methods are adopted for interpreting the developed prediction models. The probabilistic buckling stress prediction models are developed based on the trained ANN model considering the combined uncertainties of steel materials and geometries by the Latin hypercube sampling method. The GSA method is introduced for investigating the influence of the design parameters on the discreteness of the probabilistic buckling stress. Based on the achieved results, the following conclusions can be obtained:

- The ANN model can achieve the lowest value of *RMSE* (i.e., 0.0094) and the highest value of R^2 (i.e., 0.9952) within the developed ten machine learning models, demonstrating the best effectiveness of the ANN algorithm in predicting the nominal buckling stress of the SSPD.
- The probability densities of the buckling stress obtained from the developed machine learning prediction model can agree well with

that obtained from FE simulation for all considered cases, validating the accuracy and reliability of the developed machine learning prediction model.

- The nominal yielding stress of steel (f_y), the height-to-width ratio (α), the width-to-thickness ratio (β), and the initial imperfection (δ) show significant influence on the nominal buckling stress of the SSPD while the thickness of the core plate (t) shows negligible effects.
- The height-to-width ratio (α), the width-to-thickness ratio (β), and the initial imperfection (δ) have a negative relationship with the nominal buckling stress of the SSPD while the yielding stress of steel (f_y) has a positive relationship with the nominal buckling stress of the SSPD.
- The uncertainties of the yielding stress of steel (f_y) and the initial imperfection (δ) have significant influence, that of the height-to-width ratio (α) have limited influence, and that of the width-to-thickness ratio (β) and the thickness of the core plate (t) have negligible influence on the buckling stress of the SSPD.

It should be noted that the probabilistic buckling stress prediction models of steel shear panel dampers were developed based on numerical simulations in this paper and further research opportunities are provided to evaluate the reliability of the developed prediction model using test data.

CRediT authorship contribution statement

Shuling Hu: Conceptualization, Methodology, Formal analysis, Data curation, Validation, Investigation, Supervision, Writing – original draft, Writing – review & editing. **Wei Wang:** Conceptualization, Methodology, Resources, Project administration, Funding acquisition, Supervision, Writing – review & editing. **Yongchang Lu:** Formal analysis, Data curation, Investigation, Validation, Visualization.

Declaration of Competing Interest

The authors declare that they have no known competing financial interests or personal relationships that could have appeared to influence the work reported in this paper.

Data availability

Data will be made available on request.

Acknowledgment

The financial supports from the Natural Science Foundation of China (NSFC) with Grant No. 52078366 and National Key Research and Development Program of 14th Five-Year Plan of China with Grant No. 2022YFC3801904 are gratefully acknowledged. This study is also supported by the Top Discipline Plan of Shanghai Universities-Class I with Grant No. 2022-3-YB-18 and Shanghai 2022 Science and Technology Innovation Action Plan Social Development Science and Technology Research Project with Grant No. 22dz1201700.

References

[1] Hu S, Wang W, Alam MS, Ke K. Life-cycle benefits estimation of self-centering building structures. Eng Struct 2023;284:115982.
[2] Hu S, Wang W, Alam MS, Zhu S, Ke K. Machine learning-aided peak displacement and floor acceleration control of hybrid self-centering braced frames. J Build Eng 2023:106429. https://doi.org/10.1016/j.jobe.2023.106429.
[3] Hu S, Qiu C, Zhu S. Floor acceleration control of self-centering braced frames using viscous dampers. J Build Eng 2023:105944.
[4] He X, Ke K, Chen Y, Yam MC, Shao T. An experimental study of steel-concrete composite connections equipped with fuse angles. J Constr Steel Res 2022;195:107357.
[5] Ke K, Chen Y, Zhou X, Yam MC, Hu S. Experimental and numerical study of a brace-type hybrid damper with steel slit plates enhanced by friction mechanism. Thin-Walled Struct 2023;182:110249.
[6] Hu S, Zhu S. Life-cycle benefits estimation for hybrid seismic-resistant self-centering braced frames. Earthquake Engineering & Structural Dynamics 2023. https://doi.org/10.1002/eqe.3914.
[7] McDaniel CC, Uang C-M, Seible F. Cyclic testing of built-up steel shear links for the new bay bridge. J Struct Eng 2003;129:801–9.
[8] Tanaka K, Sasaki Y. Hysteretic performance of shear panel dampers of ultra low yield-strength steel for seismic response control of buildings. 12th World Conference on Earthquake Engineering, WCEE New Zealand. 2000.
[9] Nakashima M, Iwai S, Iwata M, Takeuchi T, Konomi S, Akazawa T, et al. Energy dissipation behaviour of shear panels made of low yield steel. Earthq Eng Struct Dyn 1994;23:1299–313.
[10] Xu L, Nie X, Fan J. Cyclic behaviour of low-yield-point steel shear panel dampers. Eng Struct 2016;126:391–404.
[11] Nakashima M. Strain-hardening behavior of shear panels made of low-yield steel. I: Test. J Struct Eng 1995;121:1742–9.
[12] Abebe D, Jeong S, Getahune B, Segu D, Choi J. Hysteretic characteristics of shear panel damper made of low yield point steel. Mater Res Innov 2015;19:902–10.
[13] Ma N, Lin X, Yin L, Dong X, Ou J. Mechanical properties of a novel buckling restrained shear panel damper with octagon restraining plates. Earthq Eng Struct Dyn 2022;51:259–76.
[14] Stein M, Neff J. Buckling stresses of simply supported rectangular flat plates in shear. Hampton, VA: National Aeronautics and Space Admin Langley Research Center; 1947.
[15] Gerard G. Critical shear stress of plates above the proportional limit. 1948.
[16] Wang C, Xiang Y, Chakrabarty J. Elastic/plastic buckling of thick plates. Int J Solids Struct 2001;38:8617–40.
[17] Wang C, Aung TM. Plastic buckling analysis of thick plates using p-Ritz method. Int J Solids Struct 2007;44:6239–55.
[18] Inoue T. Analysis of plastic buckling of steel plates in shear based on the Tresca yield criterion. Int J Solids Struct 1996;33:3903–23.
[19] Zhang C, Wu H, Zhu T, Lin X, Zhao J, Wang Q. Accurate prediction of shear buckling capacity of low-yield-strength steel considering plastic deformations. J Constr Steel Res 2020;172:106183.
[20] Jain S, Rai DC, Sahoo DR. Postyield cyclic buckling criteria for aluminum shear panels. J Appl Mech 2008;75.
[21] Alinia M, Habashi H, Khorram A. Nonlinearity in the postbuckling behaviour of thin steel shear panels. Thin-Walled Struct 2009;47:412–20.
[22] Gheitasi A, Alinia M. Slenderness classification of unstiffened metal plates under shear loading. Thin-Walled Struct 2010;48:508–18.
[23] Lee SC, Davidson J, Yoo C. Shear buckling coefficients of plate girder web panels. Comput Struct 1996;59:789–95.
[24] Mangalathu S, Jeon J-S. Classification of failure mode and prediction of shear strength for reinforced concrete beam-column joints using machine learning techniques. Eng Struct 2018;160:85–94.
[25] Xie Y, Ebad Sichani M, Padgett JE, DesRoches R. The promise of implementing machine learning in earthquake engineering: A state-of-the-art review. Earthq Spectra 2020;8755293020919419.
[26] Hu S, Wang W, Alam MS. Probabilistic Nonlinear Displacement Ratio Prediction of Self-centering Energy-absorbing Dual Rocking Core System under Near-fault Ground Motions Using Machine Learning. J Earthq Eng 2021;1–32.
[27] Hu S, Qiu C, Zhu S. Machine learning-driven performance-based seismic design of hybrid self-centering braced frames with SMA braces and viscous dampers. Smart Mater Struct 2022;31:105024.
[28] Hu S, Zhu S, Alam MS, Wang W. Machine learning-aided peak and residual displacement-based design method for enhancing seismic performance of steel moment-resisting frames by installing self-centering braces. Eng Struct 2022;271:114935.
[29] Hu S, Zhu S, Wang W. Machine learning-driven probabilistic residual displacement-based design method for improving post-earthquake repairability of steel moment-resisting frames using self-centering braces. J Build Eng 2022;61:105225.
[30] Hwang S-H, Mangalathu S, Shin J, Jeon J-S. Estimation of economic seismic loss of steel moment-frame buildings using a machine learning algorithm. Eng Struct 2022;254:113877.
[31] Jeon J-S, Shafieezadeh A, DesRoches R. Statistical models for shear strength of RC beam-column joints using machine-learning techniques. Earthq Eng Struct Dyn 2014;43:2075–95.
[32] Le T-T, Le MV. Development of user-friendly kernel-based Gaussian process regression model for prediction of load-bearing capacity of square concrete-filled steel tubular members. Mater Struct 2021;54.
[33] Le T-T. Practical machine learning-based prediction model for axial capacity of square CFST columns. Mech Adv Mater Struct 2020;1–16.
[34] Rahman J, Ahmed KS, Khan NI, Islam K, Mangalathu S. Data-driven shear strength prediction of steel fiber reinforced concrete beams using machine learning approach. Eng Struct 2021;233:111743.
[35] Mangalathu S, Shin H, Choi E, Jeon J-S. Explainable machine learning models for punching shear strength estimation of flat slabs without transverse reinforcement. J Build Eng 2021;39:102300.
[36] Feng D-C, Wang W-J, Mangalathu S, Taciroglu E. Interpretable XGBoost-SHAP machine-learning model for shear strength prediction of squat RC walls. J Struct Eng 2021;147:04021173.
[37] Hu S, Wang W, Lin X. Two-stage machine learning framework for developing probabilistic strength prediction models of structural components: An application for RHS-CHS T-joint. Eng Struct 2022;266:114548.
[38] Abaqus 6.18 Documentation, Dassault Systemes Simulia Corporation 2018.

[40] Alinia M, Gheitasi A, Erfani S. Plastic shear buckling of unstiffened stocky plates. J Constr Steel Res 2009;65:1631–43.
[41] Zhou W, Shi Z, Li Y, Rong Q, Zeng Y, Lin J. Elastic-plastic buckling analysis of stiffened panel subjected to global bending in forming process. Aerosp Sci Technol 2021;115:106781.
[43] Nakashima M, Akazawa T, Tsuji B. Strain-hardening behavior of shear panels made of low-yield steel. II: Model. J Struct Eng 1995;121:1750–7.
[44] Tanaka K, Sasaki Y. Study on energy absorbing performance of seismic control panel-dampers using low-yield-point steel under static loading. J Struct Constr Eng AIJ 1998;509:159–66.
[45] Liu Y, Shimoda M. Shape optimization of shear panel damper for improving the deformation ability under cyclic loading. Struct Multidiscip Optim 2013;48:427–35.
[46] Chen Z, Ge H, Usami T. Hysteretic model of stiffened shear panel dampers. J Struct Eng 2006;132:478–83.
[47] Chen S-J, Jhang C. Cyclic behavior of low yield point steel shear walls. Thin-Walled Struct 2006;44:730–8.
[48] Wang M, Fahnestock LA, Qian F, Yang W. Experimental cyclic behavior and constitutive modeling of low yield point steels. Constr Build Mater 2017;131:696–712.
[49] Xu Y, Zheng B, Zhang M. Capacity prediction of cold-formed stainless steel tubular columns using machine learning methods. J Constr Steel Res 2021;182.
[50] Rahman J, Ahmed KS, Khan NI, Islam K, Mangalathu S. Data-driven shear strength prediction of steel fiber reinforced concrete beams using machine learning approach. Eng Struct 2021;233.
[51] Mangalathu S, Shin H, Choi E, Jeon J-S. Explainable machine learning models for punching shear strength estimation of flat slabs without transverse reinforcement. J Build Eng 2021;39:102300.
[52] Kang M-C, Yoo D-Y, Gupta R. Machine learning-based prediction for compressive and flexural strengths of steel fiber-reinforced concrete. Constr Build Mater 2021;266.
[53] Kim S-H, Song X, Cho C, Lee C-H. Strength prediction of steel CHS X-joints via leveraging finite element method and machine learning solutions. J Constr Steel Res 2021;176.
[54] Le T-T, Asteris PG, Lemonis ME. Prediction of axial load capacity of rectangular concrete-filled steel tube columns using machine learning techniques. Eng Comput 2021.
[55] Liang H, Song W. Improved estimation in multiple linear regression models with measurement error and general constraint. J Multivar Anal 2009;100:726–41.
[56] Hastie T, Tibshirani R, Friedman JH. The elements of statistical learning: data mining, inference and prediction. Springer; 2009.
[58] Fan W, Chen Y, Li J, Sun Y, Feng J, Hassanin H, et al. Machine learning applied to the design and inspection of reinforced concrete bridges: Resilient methods and emerging applications. Structures 2021;33:3954–63.
[59] Cortes C, Vapnik V. Support-vector networks. Mach Learn 1995;20:273–97.
[60] Xu JG, Feng DC, Mangalathu S, Jeon J-S. Data-driven rapid damage evaluation for life-cycle seismic assessment of regional reinforced concrete bridges. Earthq Eng Struct Dyn 2022;51:2730–51.
[61] Ferreira AJ, Figueiredo MAT. Ensemble Machine Learning. Springer; 2012. p. 35–85.
[62] Feng D-C, Wang W-J, Mangalathu S, Taciroglu E. Interpretable XGBoost-SHAP machine-learning model for shear strength prediction of squat RC walls. J Struct Eng 2021;147:04021173.
[63] Kim S-H, Song X, Cho C, Lee C-H. Strength prediction of steel CHS X-joints via leveraging finite element method and machine learning solutions. J Constr Steel Res 2021;176:106394.
[64] Mangalathu S, Hwang S-H, Jeon J-S. Failure mode and effects analysis of RC members based on machine-learning-based SHapley Additive exPlanations (SHAP) approach. Eng Struct 2020;219:110927.
[65] Cakiroglu C, Islam K, Bekdaş G, Isikdag U, Mangalathu S. Explainable machine learning models for predicting the axial compression capacity of concrete filled steel tubular columns. Constr Build Mater 2022;356:129227.
[66] Lundberg S.M., Lee S.-I. A unified approach to interpreting model predictions. In Proceedings of the 31st International Conference on Neural Information Processing Systems (NIPS 2017), Long Beach, CA, 2017.
[67] Alinia M, Gheitasi A, Erfani S. Plastic shear buckling of unstiffened stocky plates. J Constr Steel Res 2009;65:1631–43.
[68] Zirakian T, Zhang J. Buckling and yielding behavior of unstiffened slender, moderate, and stocky low yield point steel plates. Thin-Walled Struct 2015;88:105–18.
[69] McKay MD, Beckman RJ, Conover WJ. A comparison of three methods for selecting values of input variables in the analysis of output from a computer code. Technometrics 2000;42:55–61.
[70] Vrouwenvelder T. The JCSS probabilistic model code. Struct Saf 1997;19:245–51.
[71] Rahman M, Okui Y, Shoji T, Komuro M. Probabilistic ultimate buckling strength of stiffened plates, considering thick and high-performance steel. J Constr Steel Res 2017;138:184–95.
[72] Shi G, Gao Y, Wang X. Material properties and partial factors for resistance of low yield point steels in China. Constr Build Mater 2019;209:295–305.
[73] Pianosi F, Beven K, Freer J, Hall JW, Rougier J, Stephenson DB, et al. Sensitivity analysis of environmental models: A systematic review with practical workflow. Environ Model Softw 2016;79:214–32.
[74] Homma T, Saltelli A. Importance measures in global sensitivity analysis of nonlinear models. Reliab Eng Syst Saf 1996;52:1–17.
[75] Saltelli A. Making best use of model evaluations to compute sensitivity indices. Comput Phys Commun 2002;145:280–97.
[76] Sobol IM. Global sensitivity indices for nonlinear mathematical models and their Monte Carlo estimates. Math Comput Simul 2001;55:271–80.
[77] Wang Meng, Sun Feifei, Yuji Koetaka, Chen Lin, Nagarajaiah Satish. Xiu-Li Du. Frequency independent damped outrigger systems for multi-mode seismic control of super tall buildings with frequency independent negative stiffness enhancement. Earthquake Engineering & Structural Dynamics 2023. https://doi.org/10.1002/eqe.3891.